

1. REPORT NUMBER CA14-2424	2. GOVERNMENT ASSOCIATION NUMBER	3. RECIPIENT'S CATALOG NUMBER
4. TITLE AND SUBTITLE Title: Development of a Rational Design Method for Shear Keys at In-Span Hinges in Multi-Frame Highway Bridges Subtitle: Part-2: Performance of Pipe Shear Key Detail		5. REPORT DATE 09/22/2014
		6. PERFORMING ORGANIZATION CODE
7. AUTHOR Kevin Zmetra, Masoud Mehr and Arash E. Zaghi		8. PERFORMING ORGANIZATION REPORT NO. NG-MRIL 14-02
9. PERFORMING ORGANIZATION NAME AND ADDRESS University of Connecticut Civil & Environmental Engineering 261 Glenbrook Road, Unit 3037 Storrs, CT 06269-3037		10. WORK UNIT NUMBER
		11. CONTRACT OR GRANT NUMBER
12. SPONSORING AGENCY AND ADDRESS California Department of Transportation Division of Engineering Services 1801 30th Street, MS #9-2/5I Sacramento, CA 95816 California Department of Transportation Division of Research, Innovation and System Information P.O. Box 942873 Sacramento, CA 94273-0001		13. TYPE OF REPORT AND PERIOD COVERED Final Report
		14. SPONSORING AGENCY CODE
15. SUPPLEMENTARY NOTES Part-1 of this report is published as a separate document.		
16. ABSTRACT Long cast-in-place post-tensioned (CIP/PS) and reinforced concrete (RC) box-girder bridges are often constructed in multiple frames separated by in-span hinges in their superstructure. In multi-frame bridges, shear key members are placed in in-span hinges to connect the adjacent frames in the transverse direction. The shear keys shall preserve the transverse seismic integrity of the bridge. Steel pipes offer several design and construction benefit as shear key elements. To this end, a shear key detail has been standardized by Caltrans, known as "pipe/cable shear key", which performs both as transverse shear key and longitudinal restrainer. However, the capacity and stiffness of this detail has not been fully investigated. This report discusses the finding from the finite element analyses performed to realize the load performance of the "pipe/cable shear key" detail. A refined three-dimension finite element model of the detail was developed using ABAQUS 6.11. The model was validated using the data from push-off experiments previously performed at the University of Nevada, Reno on a comparable detail. The force-deformation performance of the shear key detail was studied for different longitudinal gap sizes. The analyses demonstrated that: 1) the pipe shear key detail is ductile under lateral loading and is able to maintain its resistance under large transverse displacements; 2) the lateral capacity and stiffness of the pipe shear key varies with the size of the longitudinal gap; 3) cyclic loading may significantly reduce the lateral stiffness of the element; and 4) effect of variation of tensile forces in cable restrainers on the lateral resistance is negligible.		
17. KEY WORDS Multi-Frame Bridge, In-Span Hinge Shear Key, Seismic Design, Transverse Response, Pipe Seat Extender	18. DISTRIBUTION STATEMENT No restrictions. This document is available to the public through the National Technical Information Service, Springfield, Virginia 22161	
19. SECURITY CLASSIFICATION (of this report) None	20. NUMBER OF PAGES 40	21. COST OF REPORT CHARGED

DISCLAIMER STATEMENT

This document is disseminated in the interest of information exchange. The contents of this report reflect the views of the authors who are responsible for the facts and accuracy of the data presented herein. The contents do not necessarily reflect the official views or policies of the State of California or the Federal Highway Administration. This publication does not constitute a standard, specification or regulation. This report does not constitute an endorsement by the Department of any product described herein.

For individuals with sensory disabilities, this document is available in alternate formats. For information, call (916) 654-8899, TTY 711, or write to California Department of Transportation, Division of Research, Innovation and System Information, MS-83, P.O. Box 942873, Sacramento, CA 94273-0001.



Development of a Rational Design Method for Shear Keys at In-Span Hinges in Multi-Frame Highway Bridges (Part-2)

Caltrans Contract: 65A0464

Kevin Zmetra

Department of Civil and Environmental Engineering
University of Connecticut

Masoud Mehr

Department of Civil and Environmental Engineering
University of Connecticut

Arash E. Zaghi, PhD, PE

Department of Civil and Environmental Engineering
University of Connecticut

Development of a Rational Design Method for Shear Keys at In-Span Hinges in Multi-Frame Highway Bridges

(Part-2 Performance of Pipe Shear Key Detail)

Prepared for:



Caltrans

**CALIFORNIA DEPARTMENT
OF TRANSPORTATION**

Division of Engineering Service

DISCLAIMER STATEMENT

This document is disseminated in the interest of information exchange. The contents of this report reflect the views of the authors who are responsible for the facts and accuracy of the data presented herein. The contents do not necessarily reflect the official views or policies of the State of California or the Federal Highway Administration. This publication does not constitute a standard, specification or regulation. This report does not constitute an endorsement by the Department of any product described herein.

For individuals with sensory disabilities, this document is available in Braille, large print, audiocassette, or compact disk. To obtain a copy of this document in one of these alternate formats, please contact: the Division of Research and Innovation, MS-83, California Department of Transportation, P.O. Box 942873, Sacramento, CA 94273-0001.

ACKNOWLEDGEMENT

The research presented in this report was funded by the California Department of Transportation (Caltrans) Contract number: 65A0464. Special thanks are due Dr. Charles Sikorsky, the Caltrans Research Program Manager, for his significant support and advices through the project. Dr. Daryoush Tavatli, Mr. Marc Friedheim, Dr. Toorak Zokaie, Dr. Mark Mahan, Mr. Tom Ostrom and Mr. Mike Keever of Caltrans are thanked for their critical feedbacks, comments and suggestions. Dr. Saad El-Azazi is thanked for his support at early parts of the projects.

The strong support of Dr. Saiid Saiidi of the University of Nevada, Reno, and Dr. Mike Accorsi, Dr. Richard Christenson, and Dr. Sarira Motaref of the University of Connecticut is highly appreciated.

ABSTRACT

Long cast-in-place post-tensioned (CIP/PS) and reinforced concrete (RC) box-girder bridges are often constructed in multiple frames separated by in-span hinges in their superstructure. In multi-frame bridges, shear key members are placed in in-span hinges to connect the adjacent frames in the transverse direction. The shear keys shall preserve the transverse seismic integrity of the bridge. Steel pipes offer several design and construction benefits as shear key elements. To this end, a shear key detail has been standardized by Caltrans, known as “pipe/cable shear key”, which performs both as transverse shear key and longitudinal restrainer. However, the capacity and stiffness of this detail has not been fully investigated.

This report discusses the findings from the finite element analyses performed to better realize the load performance of the “pipe/cable shear key” detail. A refined three-dimension finite element model of the detail was developed using ABAQUS 6.11. The model was validated using the data from push-off experiments previously performed at the University of Nevada, Reno on a comparable detail. The force-deformation performance of the shear key detail was studied for different longitudinal gap sizes. The analyses demonstrated that: the pipe shear key detail is very ductile under lateral loading and is able to maintain its resistance under large transverse displacements; the lateral capacity and stiffness of the pipe shear key varies with the size of the longitudinal gap; cyclic loading may significantly reduce the lateral stiffness of the element; and effect of variation of tensile forces in cable restrainers on the lateral resistance is negligible.

TABLE OF CONTENT

DISCLAIMER STATEMENT	III
ACKNOWLEDGEMENT.....	IV
ABSTRACT	V
TABEL OF CONTENT	VI
LIST OF FIGURES	VII
LIST OF TABLES.....	VIII
1 INTRODUCTION.....	1
1.1 Pipe seat extender in Multi-Frame Bridges.....	1
1.2 Literature Review	2
1.3 Research Objectives	3
1.4 Methodology Overview	3
2 FINITE ELEMENT SIMULATION OF STANDARD PIPE SEAT SYSTEM.....	5
2.1 Goals of the Simulation	5
2.2 Software Platform.....	6
2.3 Geometric Model.....	6
2.4 Material Models.....	6
2.4.1 Concrete Material	6
2.4.2 Steel Material.....	10
2.5 Element Formulation.....	11
2.6 Contact Definition.....	12
2.7 Boundary Conditions and Loading Mechanism	13
2.8 Validation of the Model	14
2.9 Results and Discussion.....	16
2.9.1 Quasi-static Loading Results.....	16
2.9.2 Effect of Tensile Force in the Cables	22
2.9.3 Cyclic Loading	24
3 SUMMARY AND CONCLUSIONS	27
3.1 Summary.....	27
3.2 Observations and Conclusions	27
REFERENCES	29

LIST OF FIGURES

Figure 1.1	Pipe Seat Extenders in a Typical In-Span Hinge.....	2
Figure 1.2	Cable/Pipe Seat Extender (Caltrans, 2014)	4
Figure 2.1	Concrete Compressive Behavior	8
Figure 2.2	Steel Tensile Behavior.....	11
Figure 2.3	Meshes in the FE Model. (a) Assembly, (b) Concrete Cross-Section, (c) Main Pipe.....	12
Figure 2.4	Boundary Conditions in the Finite Element Model.....	13
Figure 2.5	Pipe-Pin Hinge Assembly, (a) Large Scale Experiment, (b) Finite Element Assembly (Zaghi & Saiidi, 2010)	14
Figure 2.6	Validation of the Pipe-Pin Hinge Finite Element Model: (a) Load Displacement Relationship, and Configuration of the Concrete Filled Pipe (b) after Large Scale Experiment and (c) after FEA (Zaghi & Saiidi, 2010)	15
Figure 2.7	Load Displacement Curves for Finite Element Quasi-Static Analysis	16
Figure 2.8	Pressure Contours (0-10 ksi) in the Concrete for 2.0-in Gap Size at Loads of (a) 260 and (b) 410 kip.....	18
Figure 2.9	Yield Stresses (Green) through the Cross-Section of the Pipe, (a) 260 and (b) 410 kip	18
Figure 2.10	Von Mises (Equivalent) Stress vs. Displacement.....	18
Figure 2.11	Progression of Von Mises Stresses in the Pipe for non-Posttensioned Configuration.....	20
Figure 2.12	Tensile Stress in Cables, No posttensioning Case.....	21
Figure 2.13	First Contact of the Inner Pipe with the Outer Pipe	22
Figure 2.14	Second Contact of the Inner Pipe with the Outer Pipe	22
Figure 2.15	Load Displacement Comparison of the Effect of Tensile Force in Cables	23
Figure 2.16	Posttension Cable Axial Stress Effects of Cyclic Loading	23
Figure 2.17	Cyclic Analysis with 2.0-in Gap Size, Non-Posttensioned Detail	24
Figure 2.18	End of Pipe (a) In Contact at Peak Load (x=3.00"), and (b) In Contact on Reload (x=2.87")	25
Figure 2.19	Concrete Damage by Cyclic Loading	25
Figure 2.20	Von Mises Stress (0-60ksi) on Pipe through Cyclic Loading: (a) initial, (b) +3.0-in, (c) 0.0-in, (d) -3.0-in, (e) 0.0-in, and (f) +3.0-in Displacement.....	26
Figure 2.21	Stress in Posttension Cables in Cyclic Analysis.....	26

LIST OF TABLES

Table 2.1 Stiffness of Non-Posttensioned Finite Element Analysis 17

1 Introduction

1.1 PIPE SEAT EXTENDER IN MULTI-FRAME BRIDGES

After the collapse of several bridges in the 1971 San Fernando earthquake due to hinge unseating, the application of cable restrainers was considered for the seismic retrofitting of existing bridges (DesRoches & Fenves, 1998). Several failures of installed restrainers in the 1989 Loma Prieta and 1994 Northridge earthquakes led to some related studies and thinking of another back up system such as pipe seat. This system has been used for both new bridges and retrofit of existing bridges as shown in Figure 1.1.

A minimum of two pipe seat extenders are positioned on the outer sides of the hinge. The pipe is typically 8" in diameter XX-strong steel pipe (un-grouted) anchored (fixed) at one end and free to slide at the other end. Sleeve in free side is a formed or cored hole enlarged to 10 inches. Sometimes, longitudinal restrainer cables are also incorporated: they are passed through the pipe and are then anchored at both ends. (Hiple, 1997). Details of pipe seat extender for new bridges are shown in Figure 1.2 (Caltrans, 2014).

Although the main purpose of pipe seat extender in multi-frame bridges is a backup for unseating, it acts as a shear key between frames and transfers shear force as well.

Therefore, conventional concrete shear key has been replaced by pipe seat as a recent change by Caltrans (Yashinsky, 2013).

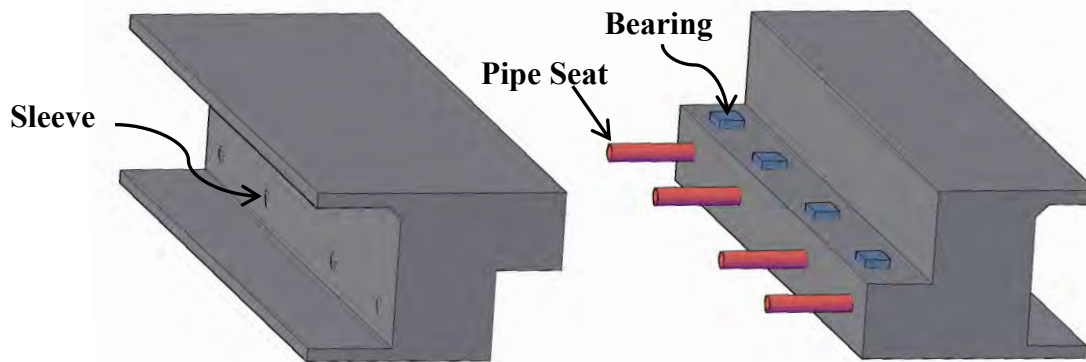


Figure 1.1 Pipe Seat Extenders in a Typical In-Span Hinge

Based on current literature, there is no reference on capacity and stiffness of pipe seat extender. Therefore, in design practice the number of pipes is determined tentatively. It is expected that gap opening affects the stiffness and capacity of pipe and may also affect the failure mode. On the other hand, the longitudinal gap is changing during an earthquake. This chapter will answer the question of pipe seat extender capacity and stiffness with consideration of longitudinal gap size effect using an analytical approach.

1.2 LITERATURE REVIEW

(Megalley, et al., 2002; Bozorgzadeh, et al., 2007) studied concrete sacrificial shear keys in bridge abutments at the component level. They developed force displacement models from experimental results, and also proposed details for ductile shear keys.

(Restrepo & Panagiotou, 2005) studied standard aerial guideway structure shear keys as part of the BART earthquake safety program. The standard aerial guideway shear key is a horizontal or vertical steel tube filled with concrete. The shear key connects the girder to a column bent cap. They tested two specimens: a 5x5x0.5" tube and a 5.0-in diameter extra-strong pipe. The test results showed that the actual capacity of the shear key is greater than those calculated theoretically, assuming pure shear yielding. Because of the large deformations imposed on the shear keys, the level of shear strains was well in excess of the yield strain. The failure mode was observed as the shear yielding of the tube. Although crushing was observed on the surface of concrete, it didn't control the capacity. They recommended using the ultimate strength

of the steel, instead of the yield strength, to calculate the shear key's capacity, and inner filled concrete's shear capacity.

(Zaghi & Saiidi, 2010) conducted an analytical and experimental study on a pipe-pin hinge system. A pipe-pin is a concrete hinge detail, which is usually positioned at the column's top and allows for the substantial reduction of moment transfer at the joint, while also providing shear strength. They concluded that the failure in pipe shear keys occurs in the concrete, but is also associated with the flexural hinging of the pipe, which depends on the geometry of the connection. Thus, the concrete failure may occur either when the concrete reaches the ultimate bearing strength or when the concrete splits because of tension or shear failure. The mode of failure, when the pipe-pin is placed in a large concrete body, is the bearing failure of the surrounding concrete.

1.3 RESEARCH OBJECTIVES

The primary purpose of this part of the study is to evaluate the stiffness and capacity of the standard pipe seat extender to serve as an in-span shear key, taking into account the effect of longitudinal gap size.

1.4 METHODOLOGY OVERVIEW

A standard pipe/cable restrainer is simulated by a finite element model using ABAQUS 6.11-1 (Dassault Systems, 2011). The full geometry of a standard pipe/cable restrainer with a limited volume of surrounding concrete is modeled. As a conservative assumption reinforcement is not modeled; according to standard drawings of the pipe seat there is no confining reinforcement around the pipe. The analysis investigated configurations with three longitudinal gap sizes: 0.0-, 2.0-, and 5.0-in, with restraining cables kept slack. The model is loaded by displacing the non-grouted block of the assembly monotonically to a displacement of 6.5 in. Two additional models with 2.0-in gap size were also analyzed. One underwent the same monotonic loading, but included initial tension in the restraining cables. This stress was set to 70% of the ultimate strength of the strand, the standard level for posttensioning strands. This is also the equivalent of the blocks sliding 1.15 in apart and is not unreasonable. The second additional model is loaded under a cyclic load to maximum displacements of +/- 3.0 in to investigate hysteresis in the detail. Aspects of the model which were investigated include load displacement behavior, initial and post-yielding stiffness, Von Mises stress evolution in the pipe, and stress level in the cables.

2 Finite Element Simulation of Standard Pipe Seat System

This chapter discusses the finite element analysis performed on the standard pipe/cable restrainer system to serve as an in-span shear key. The goals of the simulation and assumptions made in creating the model are described. The important aspects of the model are then explained, including geometry, material and element formulations, contact definitions, and boundary and loading conditions. The validation of the model with experimental data is then discussed. The chapter will conclude by presenting and discussing the results from the finite element models.

2.1 GOALS OF THE SIMULATION

The goal of the simulation is to investigate the capacity and stiffness of the standard pipe/cable restrainer system as in-span shear key considering gap size effect. The effect of gap size between concrete diaphragms is investigated in a monotonic loading scheme. The model used in the study employed a quasi-static pushover type of loading, pushing the non-grouted concrete block of the detail a total of 6.5 in. Although the cable restrainers are not posttensioned in the time of construction, one model with a 2.0-in gap size is tested with the cables under posttension stresses to simulate the tensile force due to a gap opening in a seismic event. In addition, the cyclic behavior of the detail is studied briefly. The cyclic analysis traveled through one and a quarter cycles, with peak amplitudes of +/- 3.0 in.

2.2 SOFTWARE PLATFORM

ABAQUS 6.11-1 (Dassault Systems, 2011), a finite element software capable of incorporating nonlinear materials, complex contact definitions, and large displacement nonlinearities, is utilized to model the pipe/cable restrainer. With respect to the solver methods of ABAQUS package, “Explicit Solver” performs better than the “Standard Solvers” when it comes to the high curvature contact surfaces and softening materials such as concrete. This software was chosen for the study because of its robust explicit dynamic solver, rigorous material parameters especially for concrete and outstanding contact solver methods.

2.3 GEOMETRIC MODEL

The finite element model was created in accordance with the Caltrans Bridge Standard Details introduced in Chapter 1 (Figure 1.2). The pipe is 8 xx-Strong, fixed to a head plate near the grouted end, and extends into a 10 Standard pipe as part of the fixed end assembly. Five 3/4 in nominal 7-wire post tensioning strands, $F_u = 270$ ksi, are strung between the head plates. During initial analysis, the cables were kept slack, and would only stress as the detail deformed. A second set of test were run with the cables posttensioned to $0.7F_u$, or 190 ksi. The non-grouted concrete block has a 12 in diameter opening which accepts the 8 xx-Strong pipe. Three gap sizes between the blocks were investigated: 0.0 in, 2.0 in, and 5.0 in. As a conservative assumption, concrete reinforcement was neglected.

2.4 MATERIAL MODELS

2.4.1 Concrete Material

ABAQUS/Explicit FE package has two types of nonlinear concrete material models: “Brittle Cracking” model and “Concrete Damage Plasticity” (CDP). The first one assumes a linear elastic behavior for the compressive behavior of concrete. This model is designed for cases in which concrete cracking controls the behavior. The Concrete Damage Plasticity (CDP) model includes nonlinearities in compression as well as tensile cracking. The latter one was used in this study.

The CDP model is a continuum, plasticity-based, damage model for concrete that is intended mainly for analysis of reinforced concrete structures subjected to monolithic, cyclic, and/or dynamic loading under confining pressures less than five times compressive strength of concrete. The element model assumes two failure mechanisms: (1) tensile cracking and (2) compressive crushing of the concrete material. It uses isotropic damaged elasticity in combination with isotropic tensile and

compressive plasticity to represent the inelastic behavior of concrete (Dassault Systems, 2011). The evolution of yield surface is controlled by two hardening variables, $\tilde{\varepsilon}_t^{pl}$ and $\tilde{\varepsilon}_c^{pl}$, linked to failure mechanisms under tension and compression loading, respectively.

Under uniaxial tension, the stress-strain response follows a linear elastic relationship until the tensile failure stress, σ_{to} , is reached. The failure stress corresponds to the onset of micro-cracking in the concrete material. Beyond the failure stress, micro-crack formation is represented by softening of the stress-strain response, which induces localized strain in the concrete structure. Under compression, the response is linear until the initial yield, σ_{co} , is reached. In the plastic zone, the response is typically characterized by stress hardening followed by strain softening beyond the ultimate stress, σ_{cu} . This somewhat simplified representation captures the main features of the response of concrete. It is assumed that the uniaxial stress-strain curves can be converted into stress versus plastic-strain curves. Material damage and subsequent element removal was not defined for the concrete models in this study.

Two options are offered for modeling the tensile softening behavior of concrete. The tensile material behavior can be modeled using either stress-strain or stress-displacement relationship. Displacement in the latter case represents the crack width. When stress-strain relationship is used, the smaller the size of element, the narrower the crack. By increasing the element size, the crack width increases (because crack width is equal to tensile strain multiplied by length of the element). This observation is in contrast physical behavior. For instance, in a concrete specimen developing a single tensile crack, the displacement across the crack should be independent of the specimen length. Accounting for this, the stress-displacement relationship was used for concrete in this study.

The Hillerborg's fracture energy concept was used to determine the energy required to open a unit area of crack, G_F , using "brittle fracture mechanics" (Hillerborg, et al., 1976). The area under the stress-displacement curve is equal to the fracture energy. There are several recommendations for value of G_F and shape of tensile stress-displacement curves based on experimental data (Bazant, 2002; Roesler, et al., 2007).

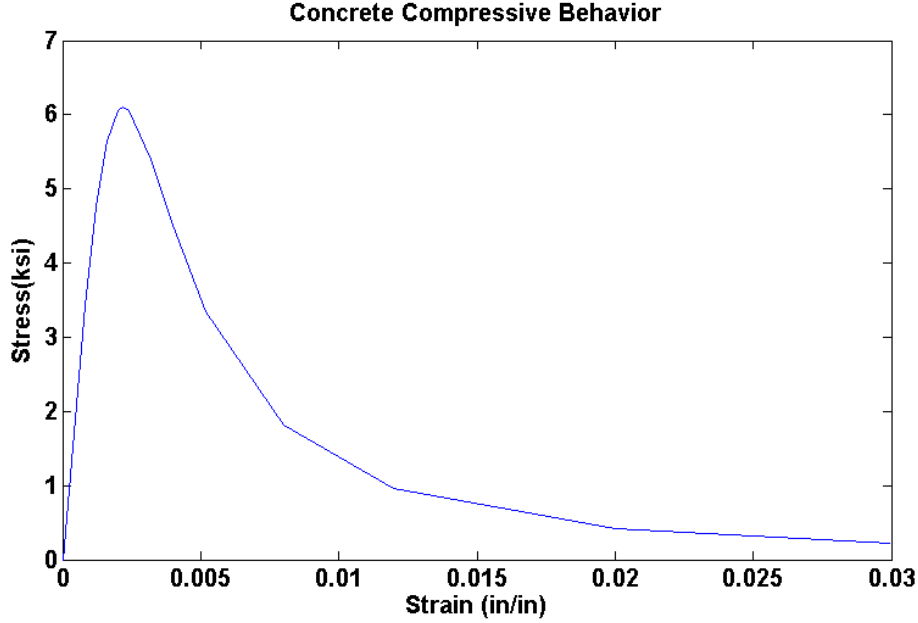


Figure 2.1 Concrete Compressive Behavior

For compressive behavior, several models have been proposed by different researchers (Babu, et al., 2005). Based on a review of these models, the Popovics (Popovics, 1973) model was used in this study, with the compressive behavior shown in Figure 2.1. In this model the compressive stress-strain relationship of concrete is determined from:

$$f_c = \frac{f'_c x^r}{r - 1 + x^r} \quad \text{Eq. 2.1}$$

where:

f'_c : is the compressive strength of the concrete

$x = \frac{\varepsilon_c}{\varepsilon_{co}}$ that, ε_{co} is the strain at maximum concrete stress of f'_c (assumed 0.002)

$$r = \frac{E_c}{E_c - E_{sec}} \quad \text{where } E_c = \begin{cases} 5000\sqrt{f'_c} & \text{(ksi)} \\ 10500\sqrt{f'_c} & \text{(MPa)} \end{cases} \quad \text{and } E_{sec} = \frac{f'_c}{\varepsilon_c} \quad \text{Eq. 2.2}$$

Note that if standard concrete cylinder is to be modeled using this curve with $\sigma_{co} = f'_c$, FE simulation of the concrete cylinder would show a different concrete strength than f'_c . The same is true for the split cylinder test result. Therefore, the values of σ_{to} and σ_{co} in the material model are different from f'_c and f_t , respectively. The values of σ_{to} and σ_{co} were tuned in the way that the analytical compressive and tensile stresses match with f'_c and f_t that were obtained from the concrete tests. As explained

earlier, only the plastic part of the strain was introduced to the program for tension and compression as defined in Eq. 2-3.

$$\tilde{\varepsilon}^p = \varepsilon - \frac{\sigma}{E} \quad \text{Eq. 2.3}$$

The CDP model assumes a non-associated potential plastic flow. The flow potential, G , that is used for this model is Drucker-Prager hyperbolic function of Eq. 2-4:

$$G = \sqrt{(\alpha \sigma_{10} \tan \psi)^2 - q^2} - p \tan \psi \quad \text{Eq. 2.4}$$

ψ : The dilation angle measured in $p-q$ plane at high confining pressure

p : Hydrostatic pressure stress $(-\frac{1}{3} \sigma_{ii})$

q : Equivalent Von Mises stress $\sqrt{\frac{3}{2} s_{ij} s_{ij}}$, where $s_{ij} = \sigma_{ij} - \delta_{ij} p$

ε : Flow potential eccentricity, default value is 0.1

A dilation angle of 37° was used in the analysis based on the literature (Fink et al., 2006).

The material model makes use of yield function proposed by Lubliner et al. (Lubliner, et al., 1989), taking into account the modifications proposed by Lee and Fenves (Lee & Fenves, 1998) to account for different evolution of strength under tension and compression. The evolution of yield surface is controlled by hardening variables, $\tilde{\varepsilon}_t^{pl}$ and $\tilde{\varepsilon}_c^{pl}$. The yield function takes the form of Eq. 2-5 in terms of effective stress.

$$F = \frac{1}{1-\alpha} (q - 3\alpha p + \beta(\tilde{\varepsilon}^p) \bar{\sigma}_{\max} + \gamma \bar{\sigma}_{\max}) - \bar{\sigma}_c(\tilde{\varepsilon}^p) = 0 \quad \text{Eq. 2.5}$$

where:

$$\alpha = \frac{(\sigma_{bo} / \sigma_{co}) - 1}{2(\sigma_{bo} / \sigma_{co}) - 1}; 0 \leq \alpha \leq 0.5 \quad \text{Eq. 2.6}$$

$$\beta = \frac{\bar{\sigma}_c(\tilde{\varepsilon}_c^p)}{\bar{\sigma}_t(\tilde{\varepsilon}_t^p)} (1-\alpha) + (1+\alpha) \quad \text{Eq. 2.7}$$

$$\gamma = \frac{3(1-K_c)}{2K_c - 1} \quad \text{Eq. 2.8}$$

$\bar{\sigma}_{\max}$: The maximum principal effective stress

σ_{bo}/σ_{co} :Ratio of initial biaxial compressive yield stress to initial uniaxial compressive yield stress (default value is 1.16)

K_c :Ratio of the second stress invariant in tensile meridian to that on the compression meridian (default value is 2/3).

The default parameters of the yield function were used in the analyses.

2.4.2 Steel Material

A bilinear plastic material stress-strain relationship was assigned to the steel materials. The material for the pipe had a yield stress of 35 ksi, an ultimate stress of 60 ksi, and a Poisson's ratio of 0.3 (AISC, 2011). Prestressing wire followed a similar bilinear behavior with yield strength of 240 ksi, ultimate strength of 270 ksi, and an elastic modulus of 25,000 ksi (ArcelorMittal, 2010). When cable tensile force was assumed, the cables were stressed to 70% of their ultimate strength, or 190 ksi, which is typical of posttensioning stress. This was chosen as a feasible maximum. Because large deformations and nonlinearities were assigned to three dimensional elements, these curves represent true stress-logarithmic strain relations. This is because as deformations become large, the cross-sectional area of the specimen decreases due to Poisson effects, increasing the localized stress. The “nominal stress-strain” curve ($\sigma_{nom} - \varepsilon_{nom}$) was transformed to “true stress-logarithmic plastic strain” relation ($\sigma_{true} - \varepsilon_{ln}$) by using Eqs. 2-9 and 2-10:

$$\sigma_{true} = \sigma_{nom}(1 + \varepsilon_{nom}) \quad \text{Eq. 2.9}$$

$$\tilde{\varepsilon}_{ln}^p = \ln(1 + \varepsilon_{nom}) - \frac{\sigma_{true}}{E} \quad \text{Eq. 2.10}$$

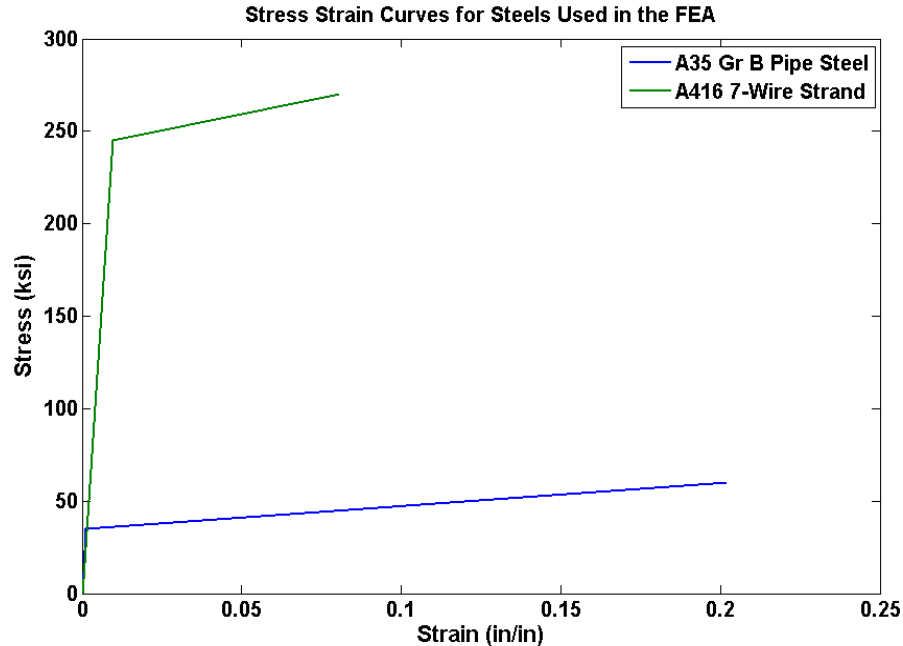


Figure 2.2 Steel Tensile Behavior

2.5 ELEMENT FORMULATION

Three dimensional linear brick elements with reduced integration (C3D8R) were chosen to model all the solid parts. The reduced integration formulation significantly reduced the computational demand without compromising the accuracy of the results. To model pretension cables, two-node three-dimensional linear truss elements (T3D2) were utilized. The truss element allows the wire to only account for axial forces and deformations. The prestressing tendon is not capable of providing any bending resistance, therefore, utilizing truss elements in lieu of beam elements is a preferable formulation. Because of the highly localized stresses induced by the posttensioning cables on the end plates, these plates were modeled as rigid.

As expected, mesh sensitivity analyses demonstrated a finer mesh is necessary in the concrete bordering the contact surface of the pipe. The tension model for the CDP concrete material depends on the third root of volume of the element (the characteristic length of element), thus, flat or narrow concrete elements were avoided in critical regions. Meshes of the assembly are shown in Figure 2.3.

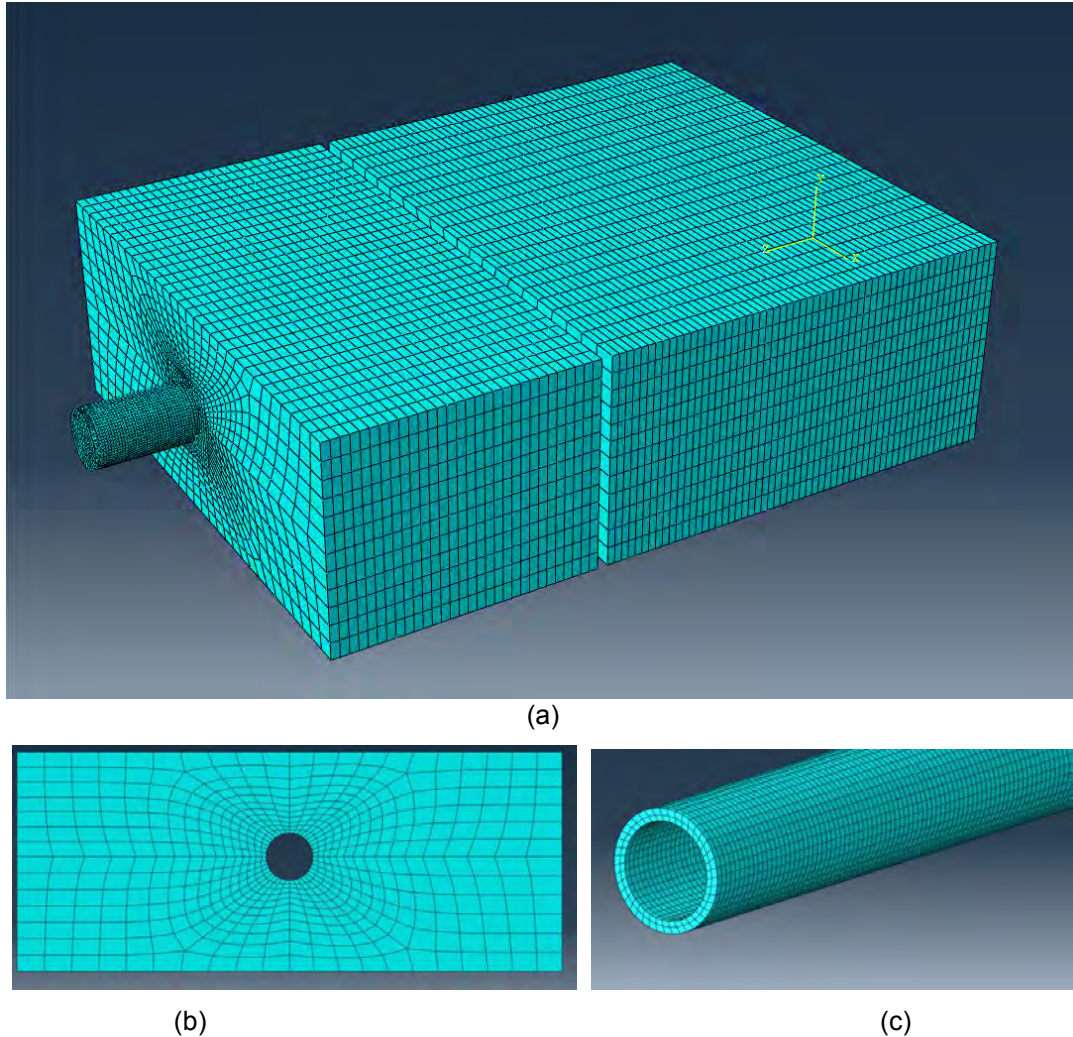


Figure 2.3 Meshes in the FE Model. (a) Assembly, (b) Concrete Cross-Section, (c) Main Pipe

2.6 CONTACT DEFINITION

Interaction between the surfaces of the steel pipe and concrete was modeled by general contact algorithm. General contact uses a sophisticated tracking algorithm to ensure that proper contact conditions are enforced efficiently.

“Hard” contact was used for the normal interaction of the contact surfaces. In this algorithm, when the surfaces are in contact, any contact pressure can be transmitted between them. The surfaces separate if contact pressure reduces to zero, but are able to come into contact again if the clearance between them reduces to zero. This contact relation is approximated by stiff linear behavior. The stiffness is adjusted automatically to minimize penetration without adversely affecting the analysis time.

The tangential interaction of contact surfaces were specified with a “Friction” model (Coulomb friction). The basic concept of the Coulomb friction model is to relate the maximum allowable friction (shear) stress across an interface to the contact pressure between the adjacent bodies. The Coulomb friction model defines the critical shear stress, τ_{crit} , at which sliding of the surfaces starts, as a fraction of the contact pressure, p , between surfaces ($\tau_{crit} = \mu p$). The coefficient, μ , was assumed to be equal to 0.425 (Baltay & Gjelsvik, 1990) (Rabbat & Russell, 1985).

In order to judge to performance of the pipe alone, contact was neglected between the concrete blocks. Tie constraints were defined to hold the parts of the fixed end assembly together. This interaction restrains the translation and rotation of one surface or node region to another. For the assembly, this can be viewed as a weld between the plates. This tie condition was also used to fix the restrainer cables to each head plate, and to fix the fixed end assembly to the concrete block.

2.7 BOUNDARY CONDITIONS AND LOADING MECHANISM

Boundary conditions were applied to each of the two concrete blocks. Fully fixed boundary conditions were imposed on four sides of each of the blocks, shown highlighted in Figure 2.4. The remaining two faces of the concrete blocks did not have boundary conditions. The loading was displacement controlled. In order to apply the pushover load, the boundary condition imposed on the non-grouted block was displaced with a constant velocity. Usually, boundary displacements are imposed using constant acceleration to reduce noise caused by impulse. Due to the gap in the ungrouted block, this noise would be present either way, so constant velocity was used to reduce computation time. A moving time average was then used in order to reduce the effects of subsequent impulsive shock and contact noise.

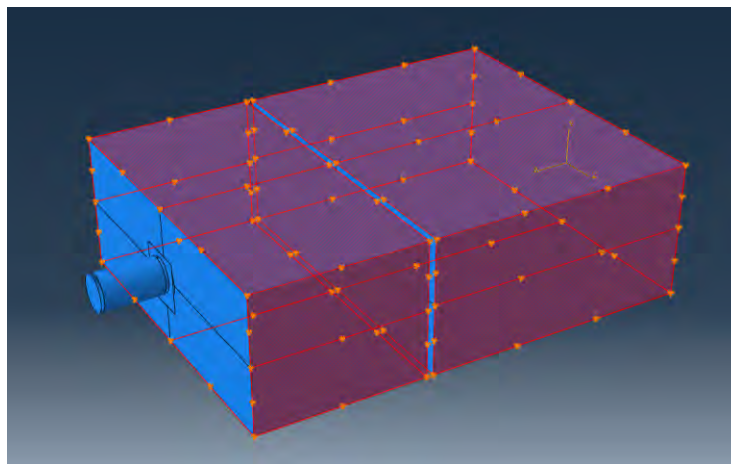


Figure 2.4 Boundary Conditions in the Finite Element Model

2.8 VALIDATION OF THE MODEL

The parameters and methodology used in this model are taken from a previously validated study on concrete filled steel pipe-pin hinges (Zaghi & Saiidi, 2010). The pipe/cable restrainer detail has very similar load transfer mechanisms and behaves similarly to the pipe-pin hinges. Using the same materials formulations, contact definitions and elements as verified by the models of Zaghi and Saiidi would provide a model which is validated for such a problem. In the investigation of Zaghi and Saiidi, large-scale experiments, Figure 2.5a, are used to create a finite element model, Figure 2.5b. The modeling methodology proved capable of demonstrating accuracy in global behaviors, such as in overall load displacement relationships, Figure 2.6a. It is also able to capture critical local behaviors, such as yielding of the pipe at both the shear interface and flexural yielding within the concrete and bearing failure of the concrete. Figure 2.6b and c show the configuration of the concrete filled pipe following the large-scale experiment and in the finite element analysis, respectively.

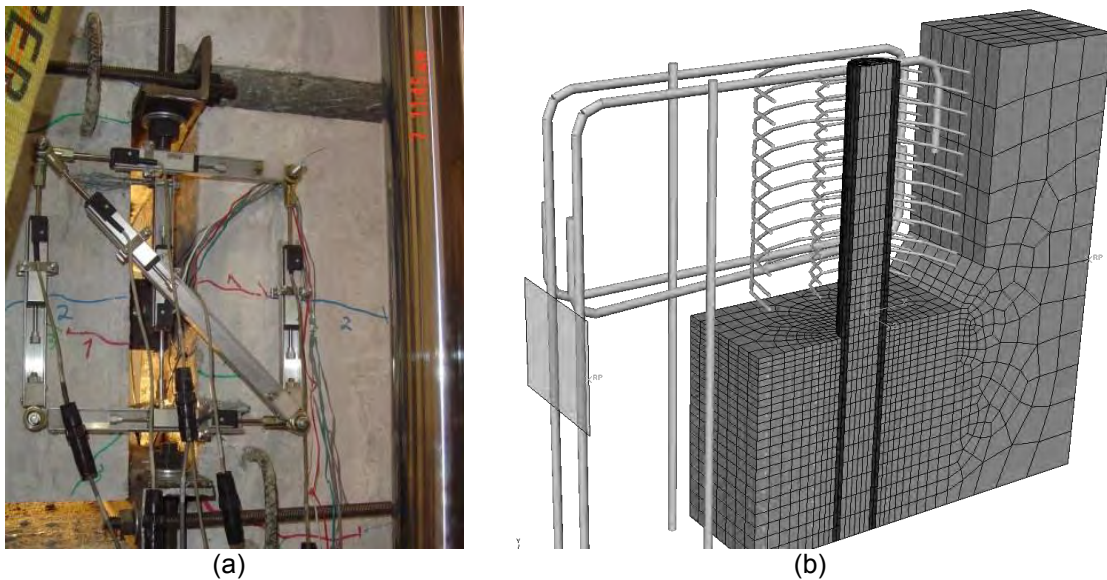
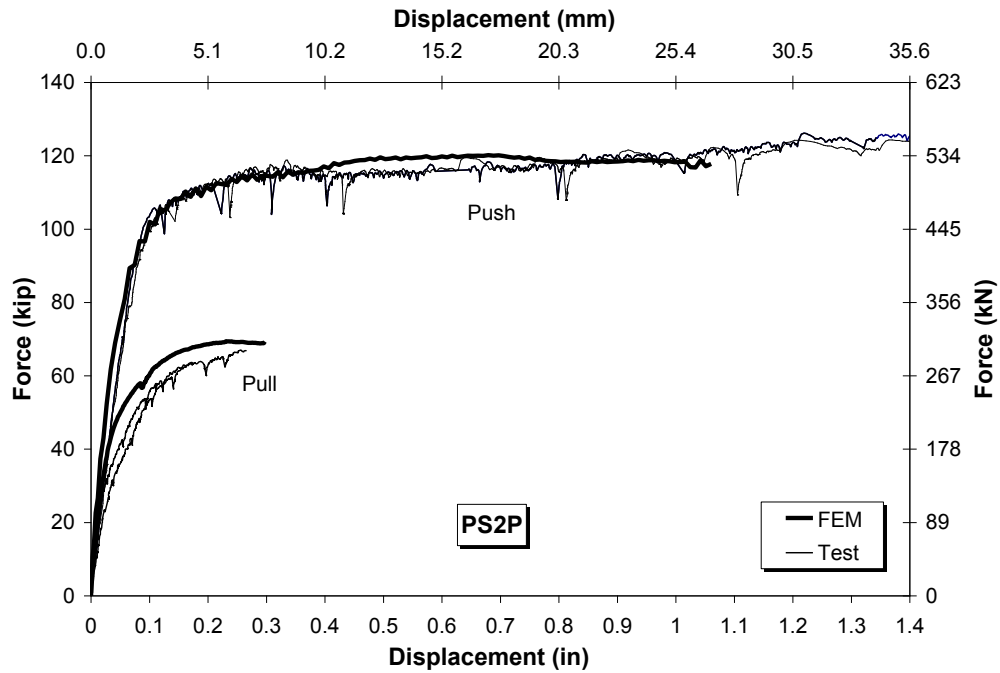


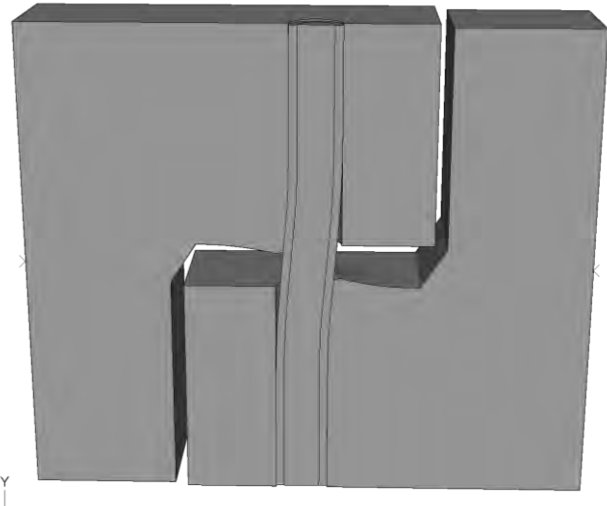
Figure 2.5 Pipe-Pin Hinge Assembly, (a) Large Scale Experiment, (b) Finite Element Assembly (Zaghi & Saiidi, 2010)



(a)



(b)



(c)

Figure 2.6 Validation of the Pipe-Pin Hinge Finite Element Model: (a) Load Displacement Relationship, and Configuration of the Concrete Filled Pipe (b) after Large Scale Experiment and (c) after FEA (Zaghi & Saiidi, 2010)

2.9 RESULTS AND DISCUSSION

Out of the finite element model, a few key aspects of the pipe/cable restrainer are investigated. The major variables of concern are the overall load displacement behavior of the detail, stiffness of both loading and post yielding, maximum stress in the pipe, and the tension in the pretension cables. Each of these provides important information about the detail. This section will first present the results of the pipe/cable restrainer with no tensile force in cables. The effects of fully posttensioning the cables on load displacement relation and pipe stresses of the specimen with a 2.0-in gap will then be presented. The section will conclude with the performance of the non-posttensioned 2.0-in gap configuration under cyclic load.

2.9.1 Quasi-static Loading Results

Figure 2.7 shows the load displacement relationship for the three non-posttensioned pushover specimens. The specimens follow the same general behavior, but a few trends become evident. The 0.71 in before initial loading is caused as the non-grouted block moves freely before the pipe contacts the fixed end assembly. This early stiffness before the pipe makes contact with the concrete is consistent between all gap sizes, having a stiffness of 46.8 kip/in.

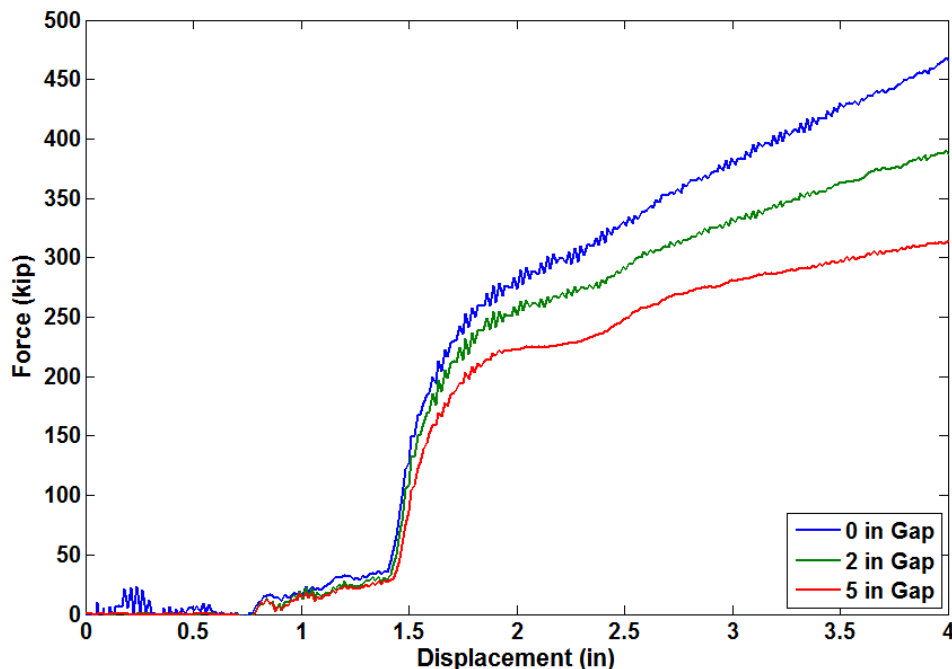


Figure 2.7 Load Displacement Curves for Finite Element Quasi-Static Analysis

The pipe then makes contact with the concrete block at a displacement of 1.42 in, and begins loading with an initial stiffness. As the size of the gap between blocks

increases, behavior is less stiff, resulting in lower loads for a given displacement, this occurs both pre- and post-yielding. The curves all begin to show initial signs of softening around a displacement of 1.65 in, caused by the onset of yielding of the pipe. As the size of the gap increases, the relationship shows yielding at lower forces due to the difference of stiffness. Yield forces of 210 kip, 190 kip and 170 kip for gap sizes of 0.0-in, 2.0-in, and 5.0-in, respectively. This lower force to yield the pipe is directly caused by an increase in the moment arm. Gap size played a significant role in ultimate capacity of the connection in the same manner. Ultimate strength of the specimens was not observed after a displacement of 6.5 in. This is caused by the large ductility of pipes under shear loading. At displacements of 6.5 in, the resistance of the 0.0-, 2.0-, and 5.0-in gap specimens were 630 kip, 490 kip, and 370 kip, respectively.

Table 2.1 Stiffness of Non-Posttensioned Finite Element Analysis

Gap Size	Initial Stiffness (kip/in)	Post-Yield Stiffness (kip/in)
0 in	1010	75.5
2 in	975	48.7
5 in	880	27.4

Initial and post-yield stiffness of each of the non-posttensioned configurations is shown in Table 2-1. Initial stiffness is defined as the slope of the load displacement curve for the first 0.1 in of displacement after contact with the concrete, while post yield stiffness is defined as the slope of the load displacement curve from 3.0 to 6.0 in. Initial stiffness decreases with increasing gap size. This is expected as a larger gap sizes creates a bending configuration that is less stiff compared to a shear configuration. After yielding, the curves continue to harden. Part of this stiffness is caused by an increase in the confining pressure in the concrete as it begins to crush. As the confinement pressure increases in the concrete, the strength of the concrete also increases since it is a pressure variant material. Figure 2.8 shows contours of concrete element pressure in the non-posttensioned 2.0-in gap size model at loads of 260 kip (a) and 410 kip (b). Crushing of the concrete is evident in Figure 2.8b, indicated in the circle. The majority of the post-yield stiffness comes from the high ductility of the round shape of the pipe. Figure 2-9 shows the deformation and spread of the yield stresses on a cut of the pipe at the interaction between the two blocks. As displacement of the non-grouted block increases, the pipe is able to fold over and collapse without rupturing. By ensuring that the pipe remains intact, post-yield hardening is able to continue.

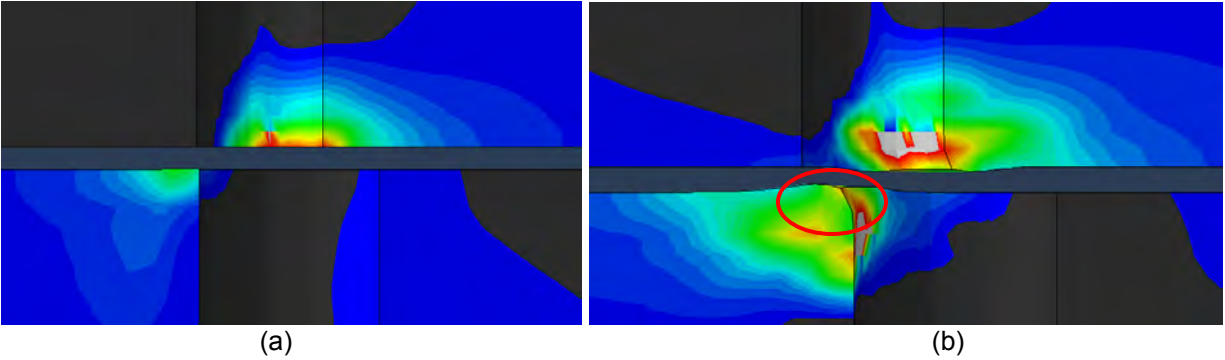


Figure 2.8 Pressure Contours (0-10 ksi) in the Concrete for 2.0-in Gap Size at Loads of (a) 260 and (b) 410 kip

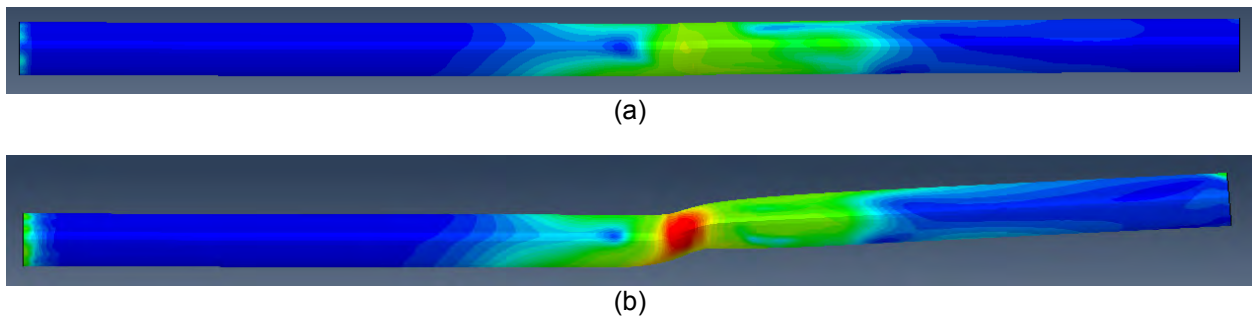


Figure 2.9 Yield Stresses (Green) through the Cross-Section of the Pipe, (a) 260 and (b) 410 kip

To judge the performance of the pipe through the pushover analysis, a plot of the Von Mises (Equivalent) Stress versus displacement is shown in Figure 2.10. This plot shows the maximum Von Mises stress in the region of the central contact around the interface of the two concrete blocks.

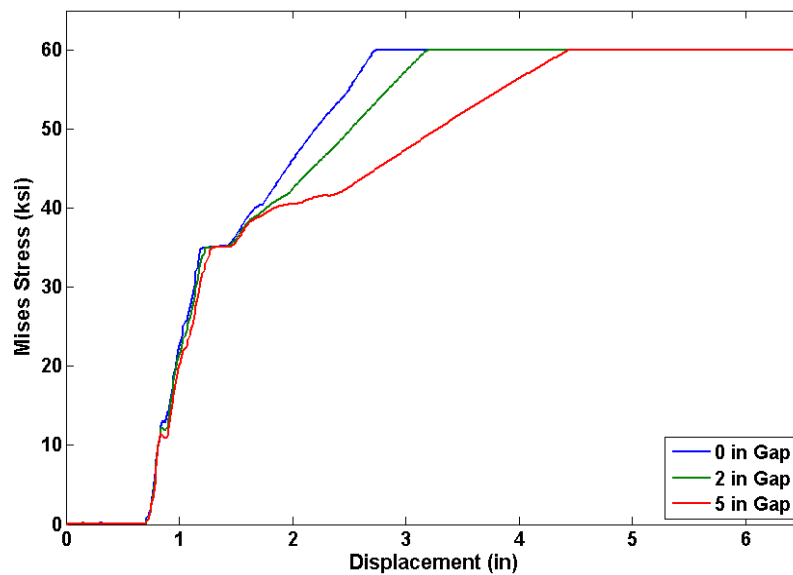


Figure 2.10 Von Mises (Equivalent) Stress vs. Displacement

Initially, it can be seen that all gap sizes behave similarly, not becoming stressed until the pipe makes contact with the fixed end assembly at 0.71 in displacement. This begins loading the pipe as a cantilever beam. After the material reaches yielding, yielding spreads through the cross section until a displacement of 1.42 in when the concrete block contacts the pipe. Figure 2.11a and b show the spread of the yield stress in the pipe with 0.0 in longitudinal gap from a displacement of 1.20 in to 1.42 in. At this point, configurations with smaller gaps increase Von Mises stresses at lower displacements compared to configurations with larger ones. During these early stages, the maximum Von Mises stress in all configurations is dominated by stress at the point of contact, and so are unaffected by gap size. Figure 2.11c shows the Von Mises plot for the 2.0 in gap pipe, showing contact dominant stress. As displacement continues, stresses in the grouted region demonstrate bending, stresses in the interface demonstrate shear, and contact stresses occur in the non-grouted block. Bending stresses are small compared to the contact and shear stresses. There comes a point when shear stresses overtake contact stresses. This point is evident in Figure 2.10 as the point of noticeable slope change in Von Mises stress. Figure 2.11d show Von Mises contours at a displacement of 2.75 in for the 2.0-in gap size pipe. Note that at this point, the maximum stress in the configuration is no longer at the initial contact point; rather the peak stress has moved 90 degrees to the top of the pipe, where shear stress would dominate. After shear stress reaches ultimate stress level, Figure 2.11e, due to the ductility of the pipe, the ultimate stress is able to spread through the pipe as it crushes (Figure 2.11f and g).

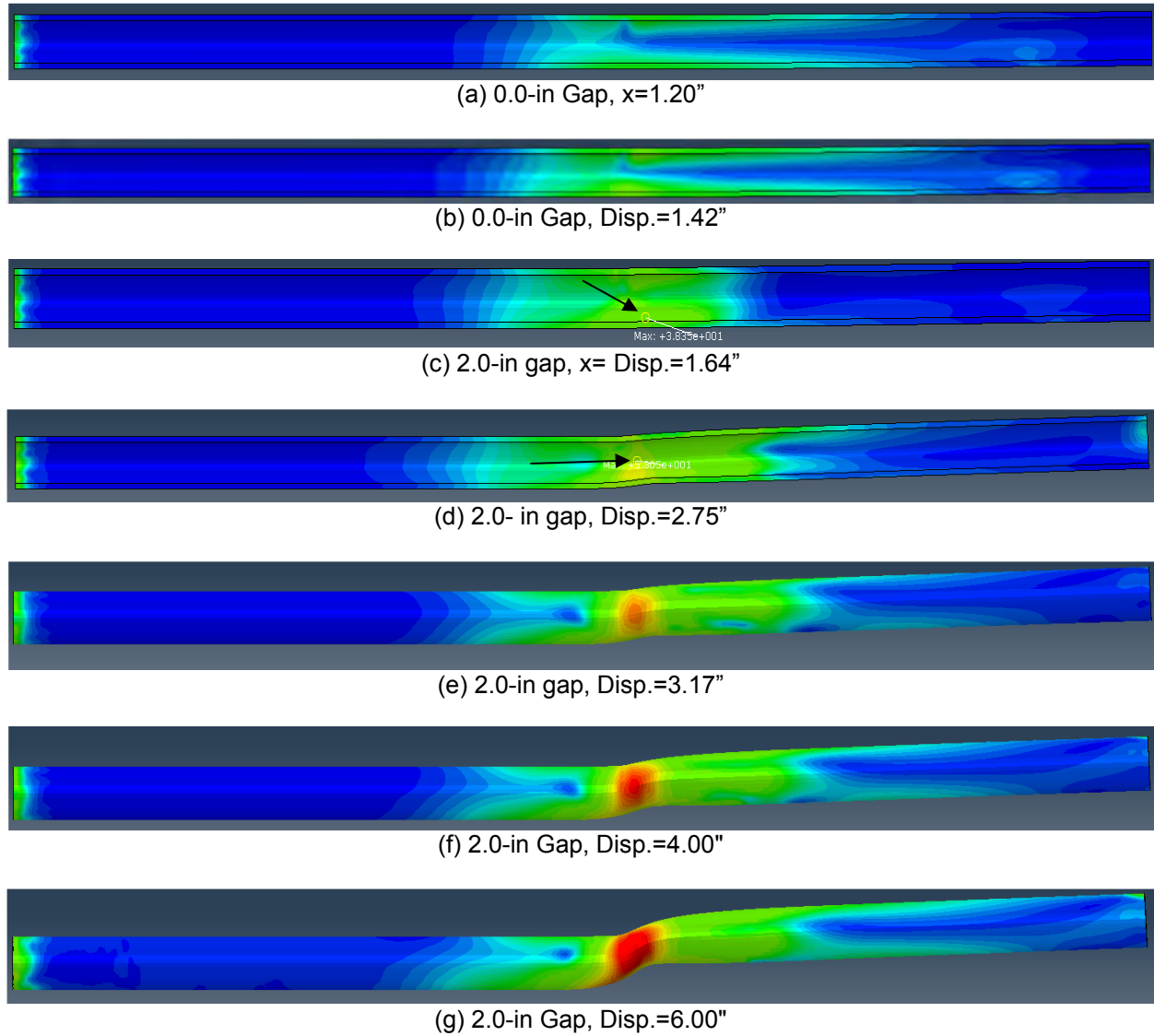


Figure 2.11 Progression of Von Mises Stresses in the Pipe for non-Posttensioned Configuration

Figure 2.12 shows a plot of axial stress in the posttension cables through the test. The size of the gap had little effect on the progression of pretension force in the cables. Configurations with smaller gap sizes gain more stress, due to the larger strain placed on the cables for the same lateral displacement. Cable stress begins to develop immediately as the cables are stretched.

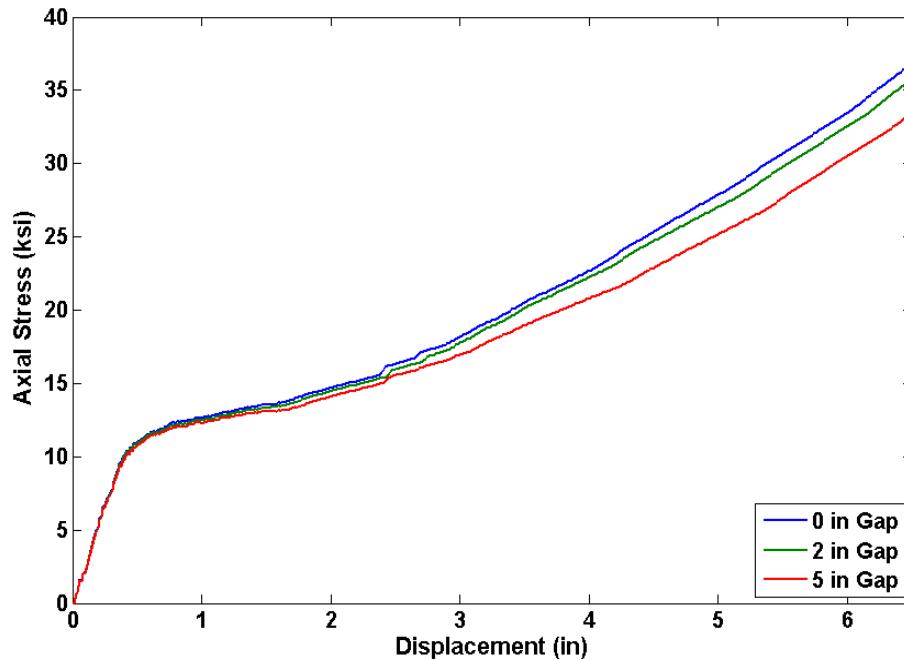


Figure 2.12 Tensile Stress in Cables, No posttensioning Case

The contact of the pipe with the fixed end assembly reduces the rate of stress gain in the cables, Figure 2.13, as the head plate is restrained from displacing with the non-grouted block. After a displacement of 2.5 in, the rate of stress gain begins, increasing again as the inner pipe contacts the other side of the fixed end assembly, Figure 2.14.

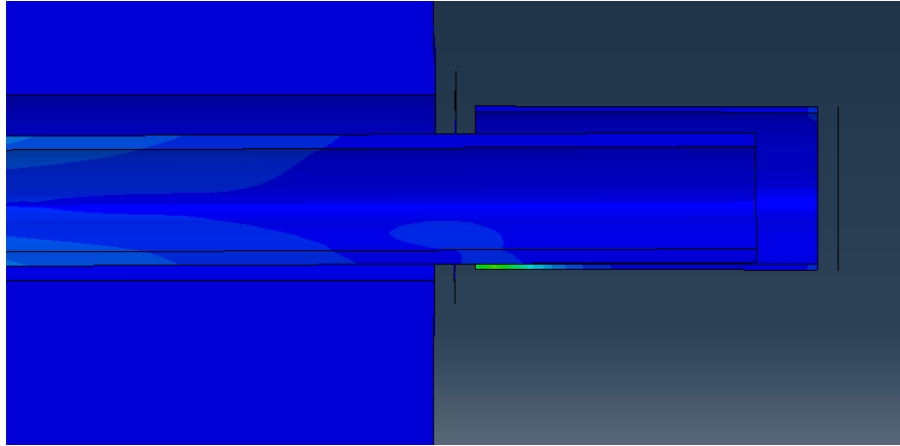


Figure 2.13 First Contact of the Inner Pipe with the Outer Pipe

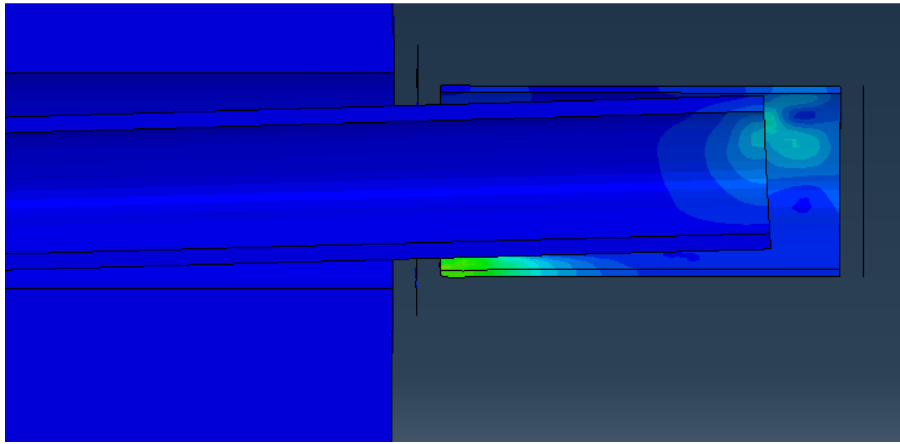


Figure 2.14 Second Contact of the Inner Pipe with the Outer Pipe

2.9.2 Effect of Tensile Force in the Cables

The presence of tensile force in the cables due to the longitudinal gap opening has no effect on the performance of the model. Figure 2.15 shows the similar load-displacement relationship for posttensioned and non-posttensioned models with 2.0-in gap size. This is expected, as the posttension cables have no way of affecting stresses in the two most critical regions, the pipe and the concrete at the points of contact. Cable stresses still progress when the cables are posttensioned, Figure 2.16. The initial loss is due to the elastic shortening as the model stabilizes. After stabilizing at 167 kip, the tension begins gaining at the nearly the same rate as the non-posttensioned case, 3.60 ksi/in compared to 4.56 ksi/in. This shows that regardless of the initial stress, level of stress gain should be expected to be equal. This could lead to rupture of the cables if a large gap develops between the blocks, causing large baseline stresses in the cables.

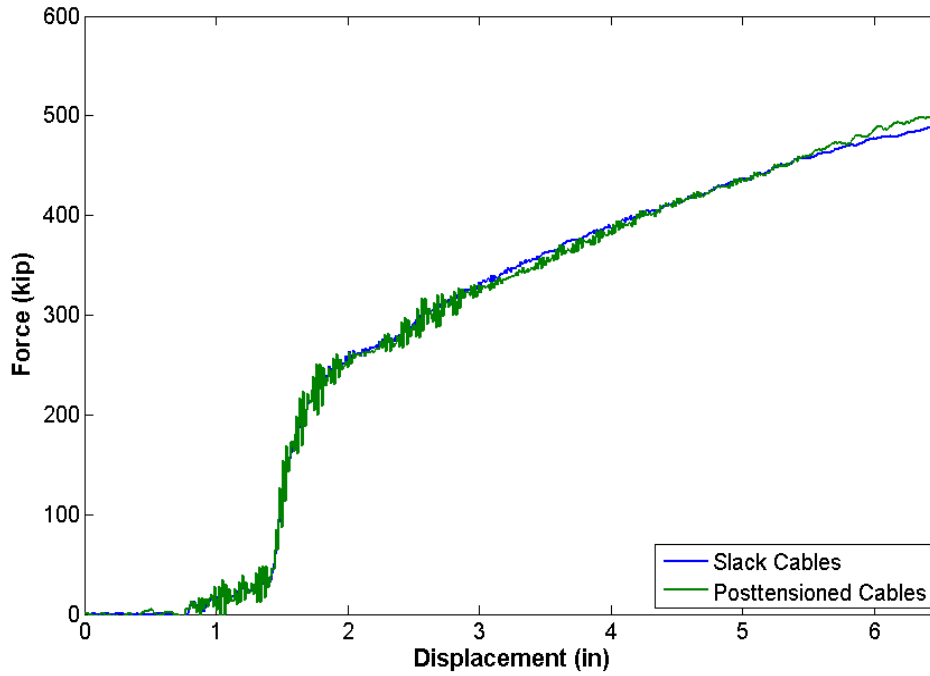


Figure 2.15 Load Displacement Comparison of the Effect of Tensile Force in Cables

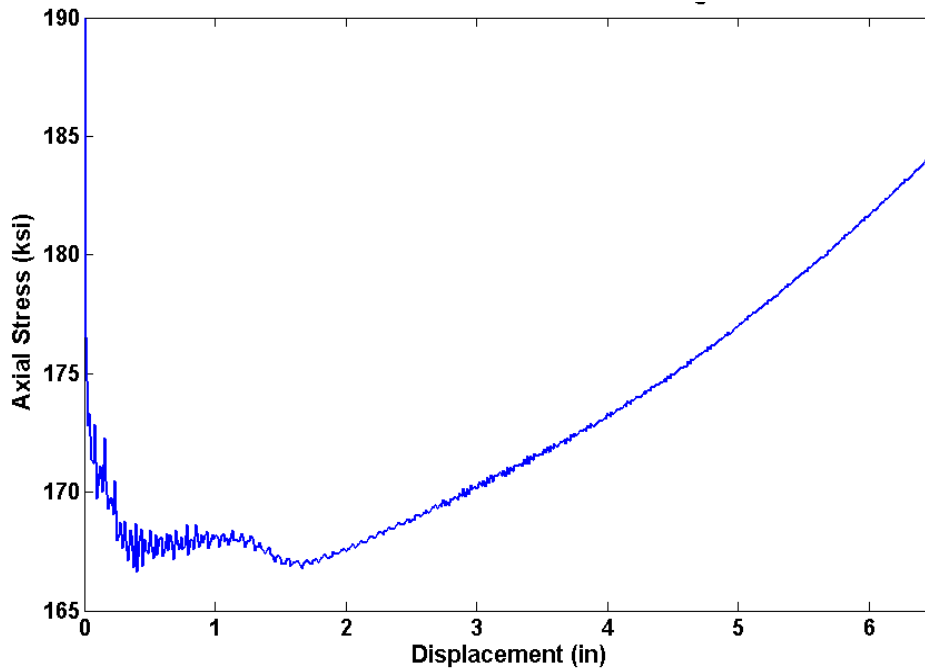


Figure 2.16 Posttension Cable Axial Stress Effects of Cyclic Loading

2.9.3 Cyclic Loading

As this detail is intended to provide functionality through a seismic event, a one and a quarter cycle analysis was performed to gain an idea of any hysterical behavior the detail may provide. Figure 2.17 shows the cyclic load displacement relationship overlaying the corresponding monotonic relationship. Peak load for the first half cycle is 329 kip. Upon unloading, the load displacement relationship unloaded extremely quickly, 2418 kip/in compared to 1010 kip/in. This high unloading rate occurs because the 8 xx-Strong pipe is already in contact with the 10 Standard pipe, and is able to begin resisting as soon as the pipe comes out of contact with the concrete, Figure 2.18.

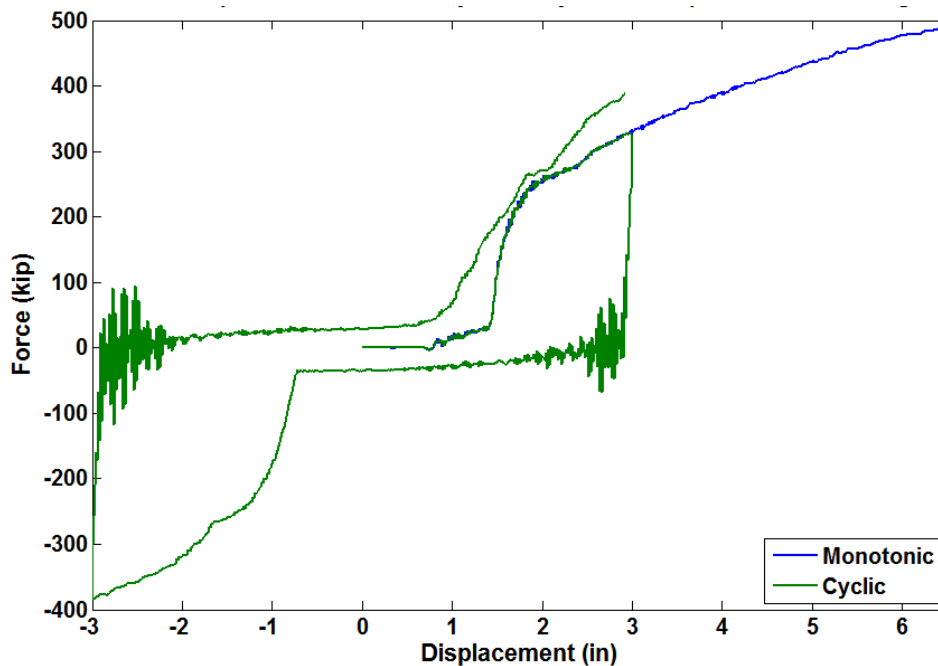


Figure 2.17 Cyclic Analysis with 2.0-in Gap Size, Non-Posttensioned Detail

Loading on the second half cycle occurred at a rate nearly half of the original undamaged loading rate, 570 kip/in. The post yielding loading rate increased 70% on the second half cycle to 83.5 kip/in; peak load on the second half cycle increased to 385 kip. Unloading rate decreased to 2135 kip/in, with loading for the last quarter cycle occurring in the same manner as after the first cycle. Loading for the last cycle behaved more like a nearly linear material, maintaining an almost constant stiffness between pre- and post-yield, 238 kip/in and 133 kip/in, respectively. Softening in the cyclic curve can be observed in the last quarter cycle around 2.5 in. This is caused by the crushing failure of the concrete, evident by the excessive bulging and concentration of equivalent plastic strain, a measure of damage, in Figure 2.19. The second cycle ultimately reached a similar load as the second half cycle, 389 kip.

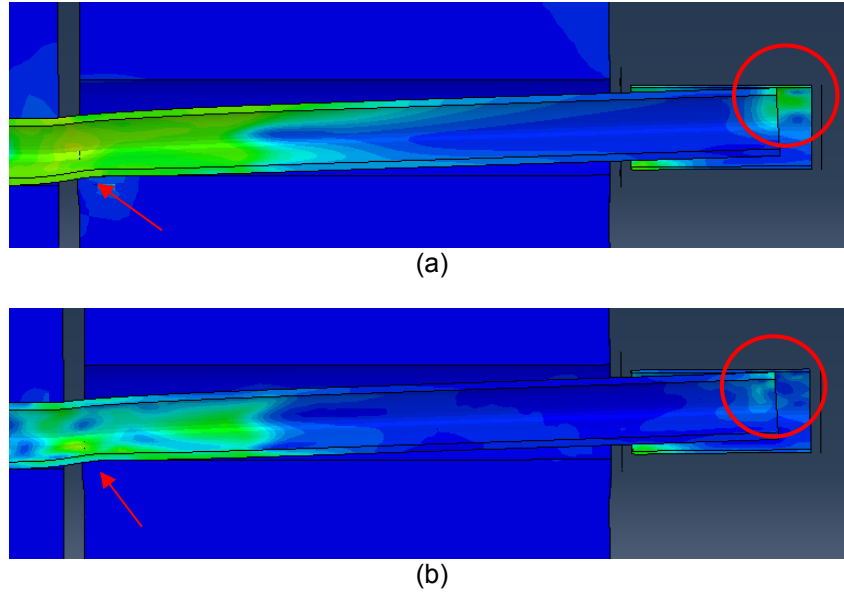


Figure 2.18 End of Pipe (a) In Contact at Peak Load ($x=3.00''$), and (b) In Contact on Reload ($x=2.87''$)

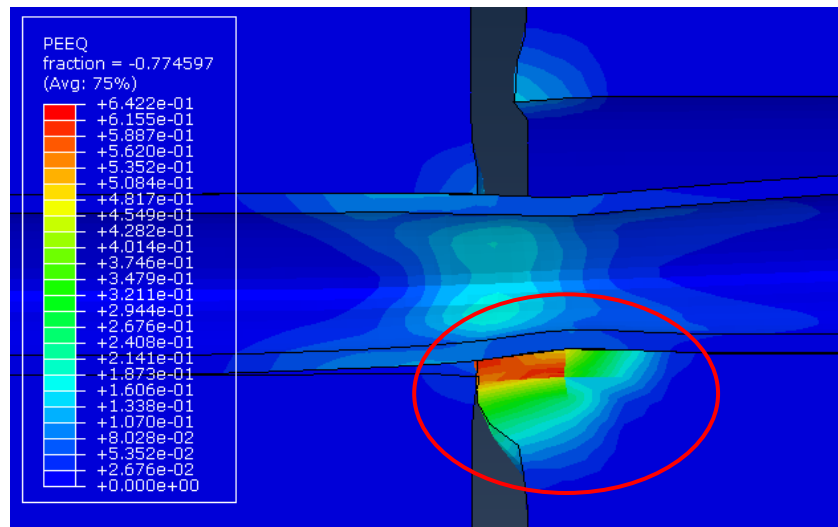


Figure 2.19 Concrete Damage by Cyclic Loading

Damage to the pipe can be seen in Figure 2.20. As the cyclic loading continues, peak stresses increase due to increasing residual stress. The pipe also begins taking a more oblong shape as permanent deformations form.

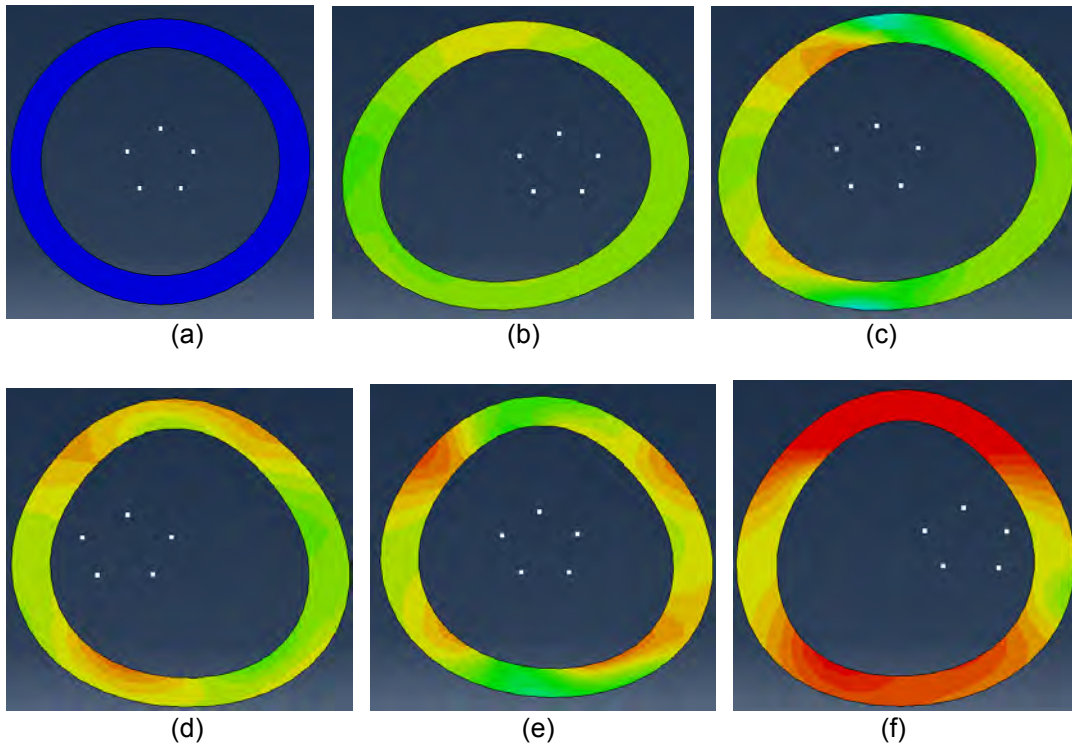


Figure 2.20 Von Mises Stress (0-60ksi) on Pipe through Cyclic Loading: (a) initial, (b) +3.0-in, (c) 0.0-in, (d) -3.0-in, (e) 0.0-in, and (f) +3.0-in Displacement

Figure 2.21 shows the behavior of the stress in the cables under cyclic loading. After completion of the first quarter cycle, the level of tension increases with each remaining cycle. Cable stress is 18 ksi after one quarter cycle, 49 ksi after three, and 71 after five quarter cycles.

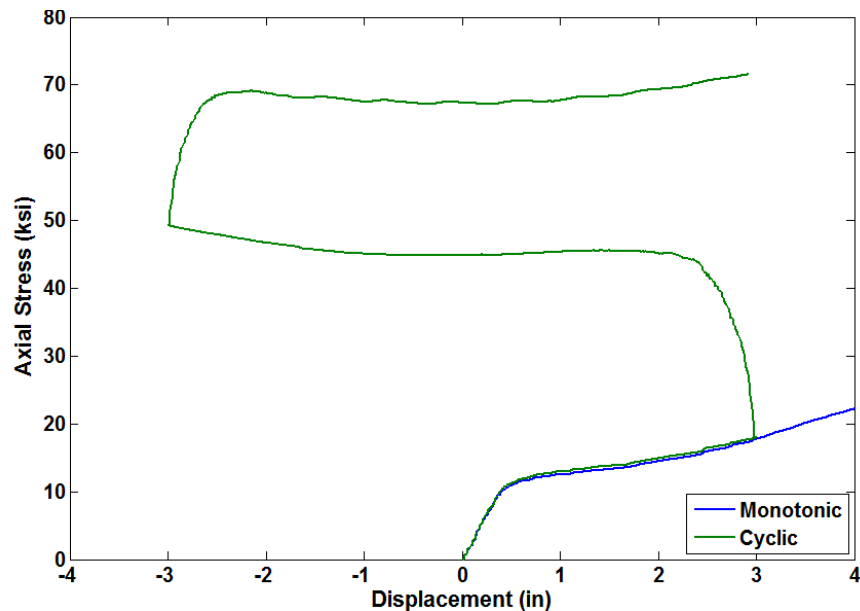


Figure 2.21 Stress in Posttension Cables in Cyclic Analysis

3 Summary and Conclusions

3.1 SUMMARY

This study was conducted to estimate performance of the standard pipe seat extender detail serving as in-span hinges shear key in multi-frame bridges. A robust finite element model of the detail was created to investigate the effect of gap size on the performance of the detail. The model was able to provide critical insight on the load displacement behavior of the model, as well as the stiffness and yield strength under varying gap sizes. Presence of tensile forces in the cables was also investigated. Monotonic loading was primarily used to load the models; however, one additional model tested under one and a quarter cycles of cyclic loading in order to investigate hysteresis response of the detail.

3.2 OBSERVATIONS AND CONCLUSIONS

Important findings of this study are concluded as:

1. The refined finite element simulation of the pipe/cable shear key detail demonstrated that the transverse yield strength, elastic stiffness, and post-yield stiffness of this detail vary by changing the longitudinal gap size. The longitudinal gap size refers to the longitudinal distance between the two concrete diaphragms in in-span hinges along the width of the bridge. The longitudinal seismic response of frames changes the longitudinal gap size. In addition, the relative in-plane rotation that occurs

between adjacent frames, due to the transverse seismic response, changes the longitudinal gap size along the width of the superstructure.

2. The “yield” strength of the 8-in xx-Strong pipe shear key detail was found to be equal to 275 kip for zero longitudinal gap size. Increasing the longitudinal gap size decreases yield capacity by 25 kip for a 2.0 in. gap size, and by 50 kip for a 5.0 in. gap size.
3. The pipe/cable shear key performs as a ductile element under quasi-static loading.
4. The effect of the longitudinal gap size on post-yield behavior of the pipe shear key detail is substantial. The post-elastic stiffnesses with 2.0- and 5.0-in. gap size were 35% and 64% smaller than that of the zero longitudinal gap size.
5. The resistance of the 8-in xx-Strong pipe shear key detail, under 6.5 in transverse displacement at in-span hinge, is 630, 490, and 370 kip for longitudinal gap sizes of 0.0-, 2.0-, and 5.0 in, respectively. It is shown in the first part of the study that the median value of the longitudinal gap size when the maximum shear key force occur is approximately 2.0 in, which is the same as the initial gap size. Therefore, for design purposes, using the yield and resistant values that correspond to the initial gap size would be justifiable.
6. Lateral plastic deformations of the pipe shear key detail is associated with yielding of the pipe section in shear. Given the large shear ductility of steel material, the pipe maintains its force resistance under large transverse displacements. No softening was observed when the in-span hinge was monolithically pushed to 6.5 in.
7. Increase in tensile forces of the cable restrainer in the pipe/cable shear key, as a result of the opening of the longitudinal gap, has negligible effects on the lateral resistance of the pipe.
8. Cyclic loading causes stiffness degradation and pinching due to local deformation of the steel pipe and crushing of the concrete at the bearing surface. The initial stiffness of the second cycle was 60% of that of the first cycle. A larger number of reversing plastic displacements may cause a larger level of stiffness and strength degradation. Further studies are necessary for a better understanding the load-deformation hysteresis response of the pipe shear key detail.

REFERENCES

- AISC, 2011. *Steel Construction Manual*. 14 ed. American Institute of Steel Construction.
- ArcelorMittal, 2010. *Prestressed Concrete Wire and Strands*. ArcelorMittal.
- Babu, R. R., Benipal, G. S. & Singh, A. K., 2005. Constitutive Modeling of Concrete: an Overview. *Asian Journal of Civil Engineering (Buildings and Housing)*, 6(4), pp. 211-246.
- Baltay, P. & Gjelsvik, A., 1990. Coefficient of Friction for Steel on Concrete at High Normal Stress. *Jorunal of Material in Civil Engineering*, 2(1), pp. 46-49.
- Bazant, Z., 2002. Concrete Fracture Models: Testing and Practice. *Journal of Fracture Mechanics*, 69, Volume 65, pp. 165-205.
- Bozorgzadeh, A., Megalley, S. H., Ashford, S. & Restrepo, J. I., 2007. *Seismic Response of Sacrificial Exterior Keys in Bridge Abutments*, La Jolla, CA: Department of Structural Engineering, University of California, San Diego.
- Caltrans, 2014. *xs7-070: Restrainer Details for Pipe Extender/Shear Key (New)*. Sacramento, CA: Bridge Standard Detail Sheets, Division of Engineering Services (DES).
- Dassault Systems, 2011. *Abaqus 6.11-1 User's Manual*. Paris: Dassault Systems.
- DesRoches, R. & Fenves, G. L., 1998. *MCEER-0013: Design Procedures for Hinge Restrainers and Hinge Seat Width for Multiple-frame Bridges*, Berkeley, California: Multidisciplinary Center for Earthquake Engineering Research (MCEER), University at California, Berkeley.
- Hillerborg, A., Modeer, M. & Petersson, P., 1976. Analysis of Crack Formation and Crack Growth in Concrete by Means of Fracture Mechanics and Finite Elements. *Cement and Concrete Research*, pp. 773-782.
- Hipley, P., 1997. *BRIDGE RETROFIT CONSTRUCTION TECHNIQUES*. Sacramento, California, SECOND NATIONAL SEISMIC CONFERENCE ON BRIDGES AND HIGHWAYS.
- Lee, J. & Fenves, G. L., 1998. Plastic-Damage Model for Cyclic Loading of Concrete Structures. *Journal of Engineering Mechanics*, 124(8), pp. 892-900.
- Lubliner, J., Oliver, J., Oller, S. & Onate, E., 1989. A Plastic Damage Model for Concrete. *International Journal of Solids and Structures*, 25(3), pp. 299-326.
- Megalley, S. H., Silva, P. F. & Seible, F., 2002. *Seismic Response of Sacrificial Exterior Keys in Bridge Abutments*, La Jolla, CA: Department of Structural Engineering, University of California, San Diego.
- Popovics, S., 1973. A Numerical Approach to the Complete Stress-Strain Curve of Concrete. *Cement and Concrete Research*, Volume 3, pp. 583-599.
- Rabbat, B. & Russell, H., 1985. Friction Coefficient of Steel on Concrete or Grout. *Journal of Structural Engineering*, 111(3), pp. 505-515.
- Restrepo, J. I. & Panagiotou, M., 2005. *BART Arial Guideway Shear Key Tests*, La Jolla, CA,: University of California, San Diego.

Roesler, J., Paulino, G., Park, K. & Gaedicke, C., 2007. Concrete Fracture Prediction Using Bilinear Softening. *Cement and Concrete Composites*, 29, 29(4), pp. 300-312.

Yashinsky, M., 2013. *Recent Change to Seismic Design Practice in California*. Sacramento, CA: Caltrans Office of Earthquake Engineering.

Zaghi, A. E. & Saiidi, M. S., 2010. *Seismic Design of Pipe-Pin Connections in Concrete Bridges*, Reno, Nevada: Center for Civil Engineering Earthquake Research (CCEER).